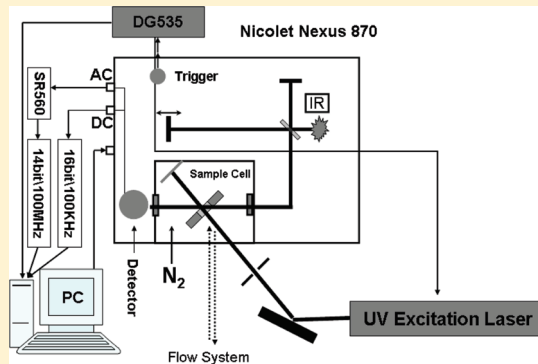


[2 + 2] Photocycloaddition Reaction Dynamics of Triplet Pyrimidines

Chunfan Yang, Youqing Yu, Kunhui Liu, Di Song, Lidan Wu, and Hongmei Su*

Beijing National Laboratory for Molecular Sciences (BNLMS), State Key Laboratory of Molecular Reaction Dynamics, Institute of Chemistry, Chinese Academy of Sciences, Beijing 100190, China

ABSTRACT: Taking the 266 nm excited pyrimidine (uracil or thymine) with cyclopentene as model reaction systems, we have examined the photoproduct formation dynamics from the [2 + 2] photocycloaddition reactions of triplet pyrimidines in solution and provided mechanistic insights into this important DNA photodamage reaction. By combining two complement methods of nanosecond time-resolved transient IR and UV-vis laser flash-photolysis spectroscopy, the photoproduct formation dynamics as well as the triplet quenching kinetics are measured. Characteristic IR absorption bands due to photoproduct formation have been observed and product quantum yields are determined to be ~0.91% for uracil and ~0.41% for thymine. Compared to the measured large quenching rate constants of triplet uracil ($1.5 \times 10^9 \text{ M}^{-1}\text{s}^{-1}$) or thymine ($0.6 \times 10^9 \text{ M}^{-1}\text{s}^{-1}$) by cyclopentene, the inefficiency in formation of photoproducts indicates competitive physical quenching processes may exist on the route leading to photoproducts, resulting in very small product yields eventually. Such an energy wasting process is found to be resulted from T_1/S_0 surface crossings by the hybrid density functional calculations, which complements the experiments and reveals the reaction mechanism.



1. INTRODUCTION

Nucleic acid bases serve as the dominant chromophores accounting for the photochemical and photophysical properties of the nucleic acids upon irradiation.¹ UV absorption of nucleic bases initially generates singlet excited states that relax rapidly to the ground electronic state primarily via ultrafast internal conversion due to the existence of conical intersections.^{1–4} By means of transient absorption spectroscopy^{5–7} or fluorescence up-conversion,^{8–10} the excited state lifetimes of nucleosides, nucleotides, and isolated bases in solution have been measured to be in the subpicosecond time range.

Despite the short lifetimes of the excited state, which is biologically relevant to the photostability of nucleic acids, photochemical damage has been observed for the monomers, oligonucleotides, and DNA upon UV radiation,^{11–13} among which the most abundant lesion is the formation of cyclobutane pyrimidine dimers (CPDs) between adjacent pyrimidine bases.^{14–17} CPD formation is believed to be a [2 + 2] photocycloaddition reaction in which the carbon–carbon double bonds of pyrimidine bases react to form a cyclobutane ring.¹⁸ The reaction process invokes the photoexcitation of a molecule to a singlet state $^1(\pi,\pi)^*$ and a triplet state by an intersystem crossing (ISC) and subsequent reaction of the excited pyrimidine base with a second molecule in the ground state. In principle, the CPD lesion could be formed via excited singlet or triplet states.

In solution, the photodimerization of single thymine bases involves a triplet state.^{19,20} A reaction via a singlet channel is precluded in this diffusion limited process because singlet excitations

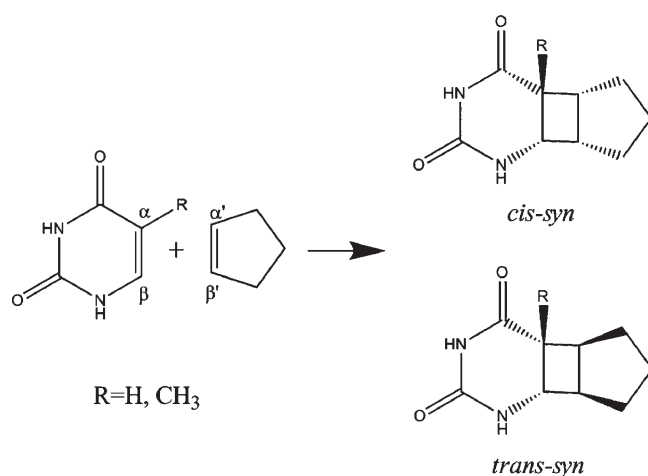
in thymine are too short-lived.^{3,21} In DNA strands, thymine bases are kept in proximity by the sugar–phosphate backbone and the diffusion limit does not apply. Although, with a short lifetime, the electronically excited singlet state may be a predominant pathway for CPD formation in a DNA strand. With femtosecond time-resolved infrared spectroscopy, Kohler and co-workers²² observed that IR marker bands specific to the *cis-syn* thymine dimer are formed less than 1 ps after excitation of single-stranded (dT)₁₈ at 266 nm. The subpicosecond formation rate of CPD strongly suggest that the reaction occurs directly from the singlet $^1(\pi,\pi)^*$ state. Furthermore, the observed ~1 ps dimerization is faster than the time scale of larger conformational changes in DNA single strands.²³ This indicates that dimerization occurs only for thymine residues that are already aligned in a reactive conformation at the instant of excitation, while the low quantum yield for CPD formation (~3%) was proposed to result from the rareness of reactive conformations in a thermal ensemble. More recently, the ultrafast formation of CPD and their yields dependent on the fraction of reactive conformers were further demonstrated by three thymine DNA model systems (TpT, (dT)₁₈, and T_LpT_L),²⁴ which shows that the propensity toward CPD formation for T_LpT_L increases significantly (by a factor of 6 with respect to TpT) because T_LpT_L adopts a C3' endo conformation that is more suitable for the thymine dimerization.

Received: February 13, 2011

Revised: April 28, 2011

Published: May 10, 2011

Scheme 1. Pyrimidine-Cyclopentene [2 + 2]
Photocycloaddition and Its Cyclobutane Product



Theoretically, CASSCF and CASPT2 calculations²⁵ indicated that the photodimerization can proceed via a barrierless concerted mechanism on a singlet excited state which is followed by the CPD formation on the ground state through an S_0/S_1 conical intersection (CI). More subtly, such a concerted singlet excited state photodimerization was suggested to be able to occur if the two neighboring thymines are at a configuration near the S_0/S_1 -CI geometry, which is certainly rare for DNA strands and thus explains the low dimerization quantum yields.

With the above elegant ultrafast experiments and high level ab initio calculations, the singlet pathway has been shown to be highly conformation restricted, which requires two bases in proximity already being stacked in a proper orientation for dimerization so that bonding can compete with ultrafast non-radiative decay. But what will happen for the excited bases without adopting a proper stacking conformation for a singlet mechanism? Aside from returning to the ground state by internal conversion, ISC through a dark doorway state $^1(n,\pi)^*$ leads to a long-lived triplet state $^3(\pi,\pi)^*$.^{26,27} The quantum yields of ISC are no greater than a few percent in aqueous solution,¹² but these long-lived states are of great importance because they can react to form CPD. More importantly, within its long lifetime, the triplet state is very likely to encounter another favorably orientated thymine residue which is brought in by the frequent conformation change of the mobile single stranded DNA²⁸ and, thus, dimerize to form CPD product. Interestingly, such a potentially important role played by the long-lived triplet state in the photodimerization reaction of single-stranded DNA has also been explored by Phillips et al.²⁹ By performing femtosecond transient absorption measurements comparatively for thymidine (dT) and (dT)₂₀, they observed a much faster T_1 decay dynamics in (dT)₂₀ (featured by ~ 140 ps time constant) than dT (with a ~ 4 ns time constant), which is a strong indication that the triplet state is chemically quenched by dimerization with an adjacent thymine base and thus becomes a major precursor for CPD formation in DNA systems. The triplet pathway for CPD formation can also gain support from theoretical calculations. A hybrid density functional calculation³⁰ finds that, in addition to the singlet excited state, the CPD formation also exhibits a favorable energy barrier along the triplet excited potential energy surface.

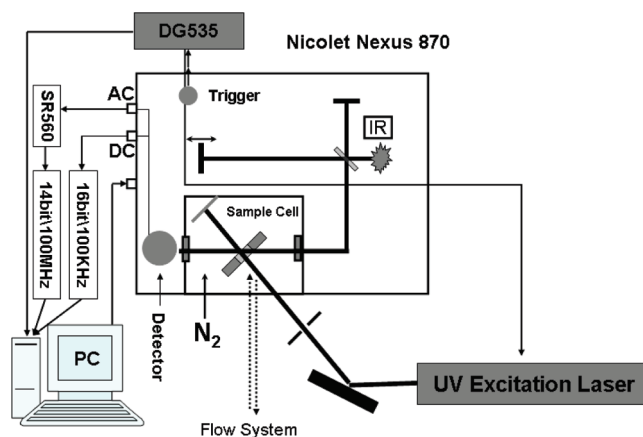


Figure 1. Schematic representation of the TR-FTIR experimental setup.

After successfully observing the ~ 1 ps CPD formation with femtosecond time-resolved infrared spectroscopy,²² Kohler and co-workers also pointed out³¹ that ultrafast CPD formation, while most readily explained by a singlet reaction, does not completely rule out a triplet state. They observed the transient infrared spectra of the lowest triplet state of thymine and thymidine³¹ at 1603 and ~ 1700 cm^{-1} due to carbonyl stretching modes. However, the CPD marker bands were not observed in this experiment for the monomeric thymine and thymidine although the residual bleaches of the parent molecules could indicate photoproduct formation. Because of the weak IR absorption and low product yields, it is difficult to probe the CPD photoproduct in the transient spectra.

To date most of the information regarding the important participation of the triplet pathway were obtained by monitoring the triplet decay dynamics or probing products with steady-state methods. Additional experimental evidence on direct photoproduct-forming dynamics is needed to provide a definitive assessment of this issue. Therefore, this paper mainly focuses on the direct observation of the photoproduct formation dynamics from the triplet state [2 + 2] photocycloaddition reactions upon the pyrimidine excitation at 266 nm. For this purpose, we choose a model system of pyrimidine (uracil and thymine) with cyclopentene (Scheme 1) due to the following reasons: (1) CPD formation is intrinsically a [2 + 2] photo cycloaddition between two carbon-carbon double bonds and the reaction of excited pyrimidine with cyclopentene can mimic this reaction process. (2) The reaction probability and product yields may be enhanced by increasing the concentration of cyclopentene as needed. Unlike the system of pure pyrimidine, the product yields are limited somehow by the poor solubility and low concentration of pyrimidine bases. (3) The cyclobutane product yielded from the excited pyrimidine reacting with cyclopentene exhibits an IR marker band at positions, which do not suffer from severe overlapping with the parent IR absorption bands. This allows the photoproduct clearly identified by transient IR spectra.

Time-resolved infrared (TR IR) spectroscopy in the nanosecond time domain is a powerful technique, which compliments conventional UV-vis laser flash-photolysis (LFP). This method becomes especially useful in detecting the DNA photoproduct formation where the absence of a UV chromophore or a low extinction coefficient of the UV absorption prevents the use of LFP. By combining the two compliment methods of nanosecond time-resolved transient IR and UV-vis LFP spectroscopy, we

have measured the photoproduct formation dynamics as well as the triplet quenching kinetics for the [2 + 2] photo cycloaddition reactions of pyrimidine (uracil and thymine) with cyclopentene. Together with hybrid density functional calculations, direct, and unequivocal information is acquired about the long-lived triplet state intermediacy possibly involved in DNA photochemistry.

2. EXPERIMENTAL AND COMPUTATIONAL METHODS

2.1. Experiments

TR-FTIR Experiments. The photoproduct formation dynamics is monitored by step-scan, time-resolved Fourier transform infrared (TR-FTIR) absorption spectroscopy.^{32,33} Step-scan FTIR spectrometers are commercially available but require significant modification for applications on flash photolysis TRIR study. The TR-FTIR instrument (setup shown in Figure 1) comprises a Nicolet Nexus 870 step-scan FTIR spectrometer, a Continuum Surelite II Nd YAG laser, a pulse generator (Stanford Research DG535) to initiate the laser pulse and achieve synchronization of the laser with data collection, two digitizers (internal 100kHz 16-bit digitizer and external 100 MHz 14-bit GAGE CS14100 digitizer), which offer fast time resolution and a wide dynamic range as needed, and a personal computer to control the whole experiment. The detector used in this work is the photovoltaic MCT (0.5 mm) equipped with a fast internal preamplifier (50 MHz).

There are two outputs from the detector: output DC, corresponding to the value of the static interferogram; and output AC, corresponding to the time-resolved change of the interferogram. The AC signal was then amplified by an external preamplifier (Stanford Research, SR560). The differential absorbance spectra are calculated based on an equation:

$$\Delta A = A_{AC+DC} - A_{DC} = -\log_{10}(1 + \Delta I_{AC}/I_{DC})$$

where I_{DC} and ΔI_{AC} are the single-beam intensity spectra corresponding to static (DC) and dynamic (AC) channels. ΔI_{AC} is calibrated before being used in equation because different gain is applied to the AC channel.^{32,33}

The fourth harmonic of Nd:YAG laser (266 nm) operating at 10 Hz repetition rate was used in the experiments. The laser excitation beam was directed through an iris aperture (1 mm in diameter) and then overlapped with the infrared beam in the sample cell within the sample compartment of the FTIR spectrometer. The laser beam energy after the aperture was 3–4 mJ per pulse. A Harrick flowing solution cell with 2 mm thick CaF_2 windows (path length: 500 μm) was used for the measurements. The closed flowing system is driven by a peristaltic pump (ColeParmer Masterflex) to refresh the sample before every laser pulse.

Laser Flash Photolysis. The triplet quenching kinetics is measured by UV–vis laser flash photolysis (LFP) with a nanosecond flash photolysis setup of Edinburgh LP920 spectrometer (Edinburgh Instruments, Ltd.), combined with a Nd:YAG laser (Surelite II, Continuum Inc.). The sample was excited by a 266 nm laser pulse (1 Hz, fwhm \approx 7 ns). The analyzing light was from a 450 W pulsed xenon lamp. A monochromator equipped with a photomultiplier for collecting the spectral range from 300 to 850 nm was used to analyze transient absorption spectra. Samples were freshly prepared for each measurement. Data were analyzed by the online software of the LP920 spectrophotometer. The fitting quality was judged by weighted residuals and a reduced χ^2 value.

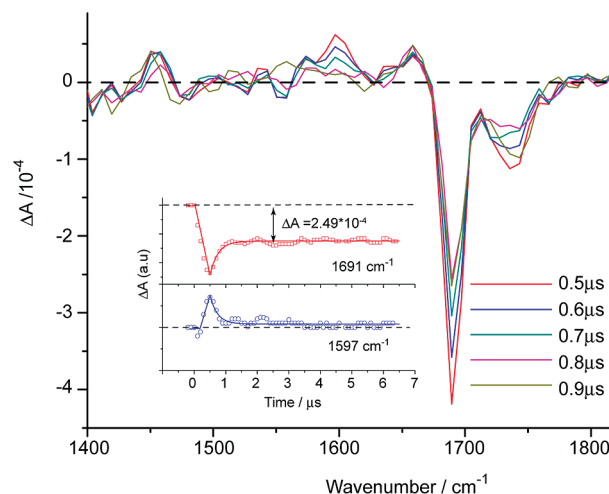


Figure 2. Infrared transient absorption spectra of 0.6 mM solution of uracil in acetonitrile- d_3 following 266 nm laser irradiation. (Note: CD_3CN is used here to obtain a broad spectral window for the detection of triplet uracil.) Inset: Kinetic traces for ground state bleach at 1691 cm^{-1} and triplet uracil formation at 1597 cm^{-1} .

Uracil (Acros Organics, 99%), thymine (Acros Organics, 99%), and cyclopentene (TCL, 98%) were used as received. Solvents of acetonitrile- d_3 (Acros Organics, 99.8%) and HPLC grade of acetonitrile were used to obtain desirable spectroscopic windows for the TR-FTIR measurements. The solutions are all saturated with Ar before and during the experiments to avoid the triplet state quenching by oxygen.

2.2. Computational Methods. For the photocycloaddition reaction of uracil or thymine with cyclopentene, the potential energy profiles along the S_0 , T_1 , and S_1 states are calculated with the Gaussian 03 program package.³⁴ The geometries of the reactants, products, intermediates, and transition states along the reaction route in T_1 or S_0 state are optimized using the hybrid density functional theory, that is, Becke's three-parameter non-local exchange functional with the nonlocal correlation functional of Lee, Yang, Parr (B3LYP) with the 6-311+G(d,p) basis sets.^{35,36} Harmonic vibrational frequencies, relative energies, and the zero-point energies (ZPE) are calculated at the same level with the optimized geometries. The intermediates are characterized by all the real frequencies. The transition states are confirmed by only one imaginary frequency. Connections of the transition states between two local minima have been confirmed by intrinsic reaction coordinate (IRC) calculations at the same level.³⁷

In parallel, the reaction pathways were also explored on the singlet excited state S_1 on the basis of TD-DFT calculations³⁸ using the S_0 stationary structures. This implementation computes vertical excitation energies only. In principle, this prevents the exact localization of stationary points on an excited-state potential energy surface. However, within the framework of the van der Lugt and Oosterhoff model³⁹ in which the geometrical features of the excited-state path are similar to those of the ground-state path, an approximate excited-state potential energy surface can be calculated using ground-state geometries.

3. RESULTS AND DISCUSSION

3.1. Photoproduct Formation Observed by TR-FTIR Absorption Spectroscopy. Figure 2 displays the TR-FTIR difference spectra of pure uracil in acetonitrile- d_3 at typical delay times

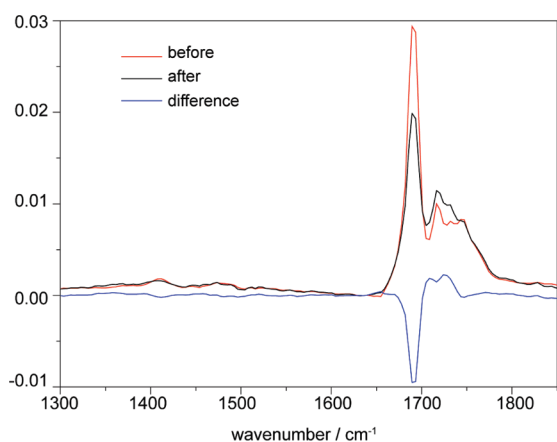


Figure 3. Steady-state IR absorption spectra of 0.6 mM solution of uracil in acetonitrile- d_3 before (red curve), after (black curve) 1 min of 266 nm laser irradiation, and the difference spectra (blue curve). The spectra were collected with a resolution of 8 cm^{-1} .

following 266 nm irradiation. Immediately after UV excitation, bleaches are observed for two ground state bands at 1691 and 1732 cm^{-1} , which correspond to the $\text{C}4=\text{O}$ (ν_6) and $\text{C}2=\text{O}$ (ν_5) carbonyl stretching modes of uracil, respectively. Meanwhile, a broad positive band at 1597 cm^{-1} appears in the transient difference spectrum. For the characteristic bands at 1691 and 1597 cm^{-1} , kinetic traces are also shown in the inset of Figure 2. These transient signals are globally fit to a single exponential decay with a lifetime of $0.60 \pm 0.10\ \mu\text{s}$. Upon oxygenation, all of the transient features disappear, which indicates that the positive band as well as the ground state bleaches is ascribed to the triplet formation. Thus, the positive band at 1597 cm^{-1} is assigned to the lowest triplet state of uracil.

In acetonitrile solution, the lowest triplet state of uracil is quenched at a rate of $2.0 \times 10^9\text{ M}^{-1}\text{ s}^{-1}$ by ground state uracil molecules.⁴⁰ When this self-quenching rate (k_{sq}) is used with our uracil concentration of 0.6 mM and the intrinsic triplet decay rate (k_0) of $5.0 \times 10^5\text{ s}^{-1}$,⁴⁰ a triplet lifetime of $0.58\ \mu\text{s}$ is calculated using the equation of $k_{\text{obs}} = k_0 + k_{\text{sq}}[\text{U}]$. The excellent agreement with the observed lifetime of $0.60 \pm 0.10\ \mu\text{s}$ from the kinetics traces in Figure 2 confirms assignment of the transient positive bands at 1597 cm^{-1} to the lowest triplet state.

For the negative bands of ground state, there is prominent residual bleach sustained at long delay times after the triplet state has decayed away (Figure 2, inset). This may indicate the formation of stable photoproduct. From the amplitude of the residual bleach at 1691 cm^{-1} , the concentration of the depleted uracil can be calculated to be $1.88 \times 10^{-3}\text{ mM}$ by $A = \epsilon c l$, where ϵ is the corresponding IR extinction coefficients of uracil. If knowing the concentration of the initially excited uracil, c^* , which is computed to be 0.19 mM based on the parameters of the UV excitation pulse, the quantum yield of uracil depletion can be obtained by $c/c^* = 0.99\%$. Assuming only photodimerization contributes to the uracil bleach, the photoproduct quantum yield ought to be half of c/c^* because two uracils form one dimer. Thus, the residual bleach actually results from a photochemical reaction with a product quantum yield of only $\sim 0.5\%$. Such a low yield is characteristic of the photodimerization of uracil upon UV irradiation in acetonitrile solution.⁴¹

Furthermore, characteristic IR bands indicative of photodimerization can be located by recording steady-state IR

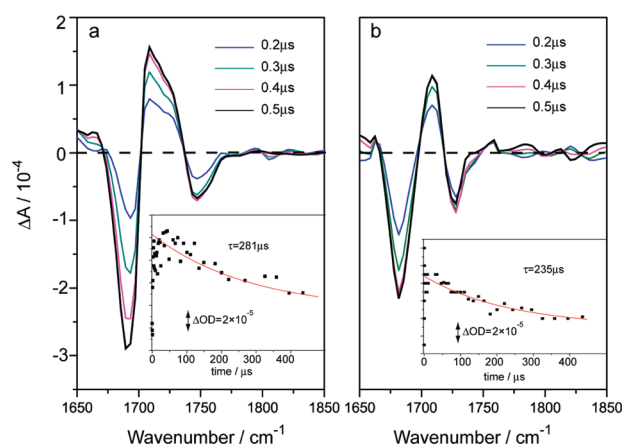
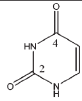
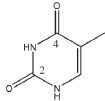


Figure 4. Infrared transient absorption spectra of a mixed solution of (a) uracil (0.6 mM) and (b) thymine (0.5 mM), respectively, with cyclopentene (0.10 M) in acetonitrile following laser irradiation of 266 nm. (Note: for the detection of photoproducts absorbing within $1650\text{--}1850\text{ cm}^{-1}$, CH_3CN is an appropriate solvent here for this spectral window.) The spectra were collected with a resolution of 16 cm^{-1} to obtain satisfactory S/N ratios. Insets: Kinetic traces for the positive photoproduct bands fitted with single-exponential decay functions.

absorption spectra before and after UV irradiation of uracil at 266 nm (Figure 3). Some fundamental vibrations of uracil are known to interact with combination or overtone vibrations due to Fermi resonances.⁴³ The resonant interaction leads to the redistribution of intensity and broadening of spectra. Thus, the broad IR bands observed in the uracil spectrum (red curve in Figure 3) contain both fundamental and Fermi resonance vibrations, including the strong carbonyl stretching (ν_5 and ν_6) bands in the $\sim 1700\text{--}1800\text{ cm}^{-1}$ range, the weak ν_8 band around 1477 cm^{-1} , and the weak ν_{10} band around 1407 cm^{-1} . In the difference IR spectrum (blue curve in Figure 3) obtained after UV irradiation, spectral changes due to photochemical reaction are only apparent in the large amplitude region above 1650 cm^{-1} , while there is no discernible changes for the weak bands below 1500 cm^{-1} . The two carbonyl stretching bands of uracil are obviously bleached, while two weak positive bands peaked at 1708 and 1725 cm^{-1} , which are the characteristic $\text{C}=\text{O}$ stretching bands of the uracil dimer,^{42,43} can be identified in between the two negative bleaching bands. This shows that uracil dimer is the only dominant photoproduct under the current experimental conditions.

However, even in the steady-state spectra (Figure 3) detecting photoproducts accumulated after 1 min irradiation, the uracil dimer only exhibits a quite weak positive band, indicating its weak IR absorption and low product yields. Because of this, none of these characteristic $\text{C}=\text{O}$ stretching bands of the CPD photoproduct can be identified in the transient difference IR spectra (Figure 2) following 266 nm pulsed irradiation of uracil. This experiment demonstrates further the difficulty of probing photoproduct from transient spectra for the pure system of pyrimidine bases in solution, due to the weak IR absorption and low product yields of CPD as reported for the system of thymine.³¹ Meanwhile, it shows that the photodimerization of uracil itself is not expected to interfere with the detection of both the transient species and the photoproducts, because, on one hand, the uracil dimer does not generate any signals in the transient IR spectra, and on the other hand, in the mixed system of uracil with large excess of cyclopentene, the photodimerization of uracil itself

Table 1. B3LYP/6-311+G(d,p) Calculated IR Frequencies and Intensities for the Carbonyl Stretching Modes in Uracil, Thymine, and their Cyclobutane Photoproducts

		$\nu(\text{C}=\text{O})$ cm^{-1}	IR intensity km mol^{-1}	ϵ $\text{M}^{-1}\text{cm}^{-1}$	$\nu(\text{C}=\text{O})$ cm^{-1}	IR intensity km mol^{-1}	ϵ $\text{M}^{-1}\text{cm}^{-1}$
Uracil		1732	661.59	-	1699	791.83	2647 ^a
Uracil+cyclopentene photoproduct	Trans-syn(P1)	1712	773.05	2584.22 ^b	1700	435.49	1455.79 ^b
	Cis-syn(P2)	1712	736.39	2461.67 ^b	1697	364.59	1218.78 ^b
Thymine		1729	808.11	-	1685	653.17	4160 ^c
Thymine+cyclopentene photoproduct	Trans-syn(P1)	1717	796.80	5074.77 ^d	1695	357.98	2279.95 ^d
	Cis-syn(P2)	1712	753.45	4798.68 ^d	1690	309.38	1970.42 ^d

* The harmonic vibrational frequencies are scaled by a factor of 0.96. Corresponding IR extinction coefficients ϵ are also listed. ^{a,c} These values are estimated according to the measured steady state IR absorption spectrum of uracil or thymine in acetonitrile. ^{b,d} The extinction coefficients of photoproducts are estimated by comparing their IR intensities with those of the uracil or thymine, based on the fact that the IR intensities are proportional to the corresponding extinction coefficients.

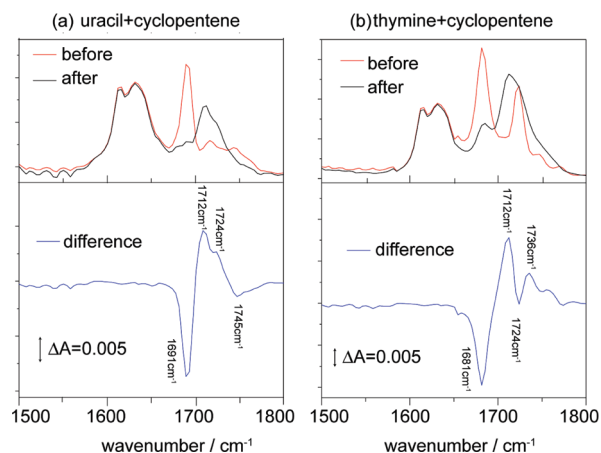


Figure 5. Steady-state IR absorption spectra of a mixed solution of (a) uracil (0.6 mM) and (b) thymine (0.5 mM), respectively, with cyclopentene (0.10 M) in acetonitrile- d_3 recorded before and after 1 min of 266 nm irradiation; The corresponding difference spectra (blue curves) are plotted in the lower panels. The spectra were collected with a resolution of 8 cm^{-1} .

can not compete with the photocycloaddition of uracil with cyclopentene.

For the solution of uracil mixed with large excess of cyclopentene, obvious photoproduct formation is observed in the transient IR spectra upon 266 nm excitation. Compared to the large molar extinction coefficient of uracil ($\epsilon = 8000 \text{ M}^{-1}\text{cm}^{-1}$),⁴⁴ cyclopentene ($\epsilon = 0.056 \text{ M}^{-1}\text{cm}^{-1}$)⁴⁵ simply does not absorb 266 nm. Only uracil is excited by 266 nm in the mixed system, leading to the observed photoproducts. As shown in Figure 4a, a broad positive band with two peaks partially resolved at 1712 and 1724 cm^{-1} can be clearly identified, which grow in between the two ground state bleaches from 0.2 to $0.5 \mu\text{s}$. This reflects the gradual forming process of the photoproducts from a bimolecular reaction. Unlike the triplet, which decays fast with a lifetime of $0.6 \mu\text{s}$, the bands at 1712 and 1724 cm^{-1} decay slowly at several hundreds of μs due to the diffusion out of the observation

zone, with a lifetime of $281 \mu\text{s}$, as shown in the Figure 4a, inset. This indicates that the newly formed positive band arises from the stable photoproduct of uracil with cyclopentene, which is a cyclobutane adduct, as indicated in Scheme 1. Vibrational frequencies for these cyclobutane adducts were calculated at the B3LYP/6-311+G(d,p) level and are given in Table 1. According to the calculation, the cyclobutane adduct has two conformations, *trans-syn* and *cis-syn*. The calculated vibrational frequencies of two carbonyl stretching are 1712 and 1700 cm^{-1} for the *trans-syn* adduct and 1712 and 1697 cm^{-1} for *cis-syn* adduct. Compared to the observed photoproduct frequencies at 1712 and 1724 cm^{-1} , the calculated values are red-shifted by 12 cm^{-1} . Thus, the photoproduct band at 1712 and 1724 cm^{-1} can be confidently assigned to the two carbonyl stretching modes of the cyclobutane adduct of uracil with cyclopentene. To solidify this assignment, steady-state IR absorption spectra of uracil with cyclopentene were also recorded before and after 266 nm irradiation (Figure 5a). The spectra before UV exposure (red curve) shows both the C=C stretching bands of cyclopentene at $\sim 1630 \text{ cm}^{-1}$ and the C=O stretching bands of uracil at ~ 1691 and $\sim 1745 \text{ cm}^{-1}$. After 1 min of 266 nm irradiation, the uracil bands are strongly bleached and two positive bands at ~ 1712 and $\sim 1724 \text{ cm}^{-1}$ are observed prominently, which is characteristic of the formation of the stable photoproduct, that is, the cyclobutane adduct of uracil with cyclopentene. The two positive IR bands observed in the TR-FTIR spectra match those present in the steady-state spectra, confirming further their assignment to the stable photoproduct, but not transient species.

If comparing Figure 5a with Figure 3, it can be seen that the IR absorption for the cyclobutane adduct of uracil with cyclopentene is much stronger than that for the uracil dimer, although the carbonyl stretching bands of these two photoproducts fall within identical spectral region around 1700 cm^{-1} . This is in agreement with the observation from Figure 2 and Figure 4a, which shows that the cyclobutane adduct of uracil with cyclopentene can be explicitly observed, but the uracil dimer is invisible in the transient IR spectra. The cyclobutane adduct of uracil with cyclopentene might have larger product yields and stronger IR absorption than those of the uracil dimer, making it possible to

detect photoproducts in transient IR spectra for the reaction system of uracil with cyclopentene, but not for pure uracil systems.

For the analogous photochemical system of thymine with cyclopentene, the cyclobutane adduct featured by a positive band at 1712 cm^{-1} is also observed in the transient IR spectra, as shown in Figure 4b. After fast formation within $0.5\ \mu\text{s}$, this band sustains its intensity and decays slowly, with a lifetime of $235\ \mu\text{s}$, corresponding to the stable photoproduct. The vibrational frequencies of two carbonyl stretching modes calculated at the B3LYP/6-311+G(d,p) level are 1717 and 1695 cm^{-1} for the *trans-syn* adduct and 1712 and 1690 cm^{-1} for *cis-syn* adduct. The separation between the two carbonyl stretching bands is both 22 cm^{-1} for these two stereoisomers. However, only a single IR positive band is observed for the photoproduct near 1712 cm^{-1} in the photochemical system of thymine in the TR-FTIR spectra. This is ascribed to the reason that the other positive IR band separated 22 cm^{-1} apart from the 1712 cm^{-1} band is masked by the negative bleaching band of thymine and, thus, can not stand out as a positive band in the transient spectra. Even in the steady-state difference spectra of thymine with cyclopentene recorded before and after 266 nm irradiation (Figure 5b), there is only one prominent positive band observed at 1712 cm^{-1} . The other band at 22 cm^{-1} away is buried mostly inside the negative bleaching band of thymine at 1724 cm^{-1} , making the net absorption of the bleaching band at 1724 cm^{-1} sustained above zero. There is only a weak leftover of this second positive band, which can be discerned at 1736 cm^{-1} in the steady-state spectra, while in the TR-FTIR spectra, which records only small amount of photoproducts after a single laser shot, such a weak second band can not be observed at all. As a result, there is only one IR band, the strong band at 1712 cm^{-1} , observed for the photoproduct from the photochemical system of thymine in the TR-FTIR spectra. This is unlike the photochemical system of uracil with cyclopentene, for which it happens that the two carbonyl stretching bands of the photoproduct are only $\sim 12\text{ cm}^{-1}$ apart and both falling in between the two negative bleaching bands of uracil, making it possible to observe both of these two IR bands of the photoproducts in either the TR-FTIR spectra (Figure 4a) or the steady-state spectra (Figure 5a).

With the above TR-FTIR experiments, characteristic IR absorption bands due to photoproduct formation have been observed. The product quantum yields can be determined if knowing the IR extinction coefficient with the method reported in literature.²⁴ The IR absorption intensity ought to be given by

$$\Delta A(\nu) = \Delta \varepsilon(\nu) \times c^* \times d \times \varphi_q$$

Here, c^* is the concentration of the initially excited molecules (uracil or thymine), $\Delta \varepsilon(\nu)$ is the wavenumber dependent difference between the IR extinction coefficient of photoproduct (cyclobutane adduct) and reactant (uracil or thymine), d is the path length of the IR cell, which is identical (0.5 mm), and φ_q is the product quantum yields. The IR extinction coefficients of the relevant species are listed in Table 1. The extinction coefficients of the reactant (uracil or thymine) were obtained from its steady-state FTIR spectra. By comparing the B3LYP/6-311+G(d,p) calculated IR intensities (also listed in Table 1), which are proportional to their corresponding extinction coefficients, extinction coefficients of various photoproducts can be determined. Meanwhile, the concentration c^* was computed based on the parameters of the UV excitation pulse (its energy, its diameter at the sample location, and its absorption by sample), which is

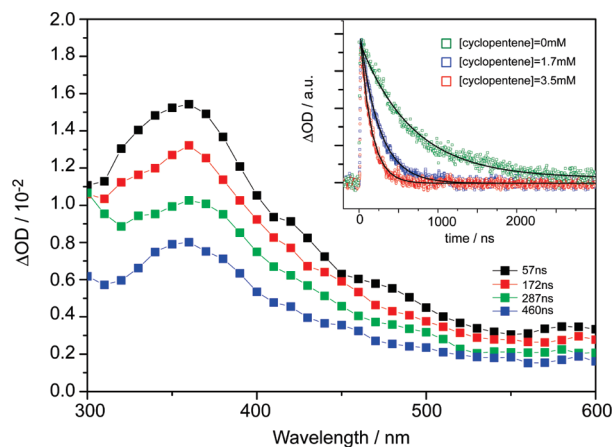


Figure 6. Transient UV–vis absorption spectra of 0.6 mM uracil in acetonitrile obtained at typical delay times after the 266 nm laser excitation. Inset: temporal profiles of the triplet uracil at 360 nm in the presence of different cyclopentene concentrations.

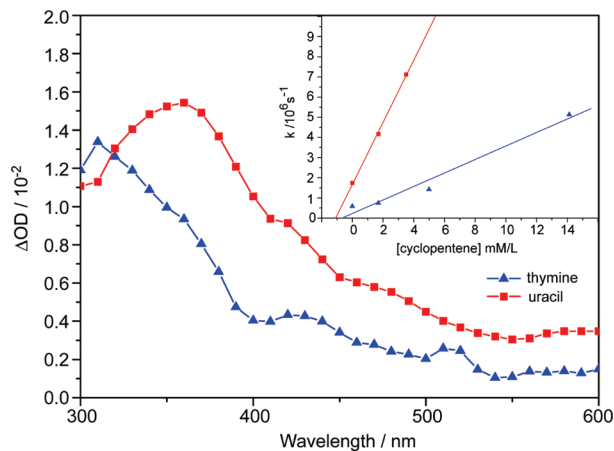


Figure 7. Transient UV–vis absorption spectra of uracil (red color) and thymine (blue color) in acetonitrile immediately after the 266 nm laser excitation. Inset: the observed triplet quenching rates as a function of cyclopentene concentration for uracil (red color) and thymine (blue color).

0.19 mM for uracil and 0.16 mM for thymine. Finally, the absolute quantum yields φ_q are estimated to be $\sim 0.91\%$ for uracil and $\sim 0.41\%$ for thymine. Our observation from time-resolved experiments is consistent with the product yields obtained from previous steady-state irradiations.^{41,46}

Compared to uracil + cyclopentene, the photoproduct quantum yields of thymine + cyclopentene are smaller by a factor of ~ 2.2 . This consists with the lower triplet quantum yield of thymine (0.06) than uracil (0.2) in acetonitrile.⁴⁰ Furthermore, the photoproduct yields were significantly lowered upon oxygenation, for both the photochemical system of uracil + cyclopentene and thymine + cyclopentene. These results clearly suggest that the photoinduced cycloaddition reaction of uracil (or thymine) with cyclopentene occurs through the T_1 state in dilute solution. The triplet state is the major precursor of the cyclobutane adduct. This finding agrees with previous proposition that in solution the photodimerization of single thymine bases involves a triplet state, but not a singlet state because singlet

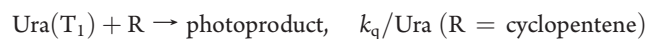
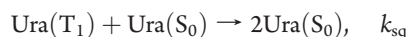
excitations are too short-lived to be subject to bimolecular reaction in this diffusion limited process.^{19–21}

3.2. Triplet Quenching Kinetics Measured by Transient UV–Vis Absorption Spectroscopy. With the above TR-FTIR experiments, the photoproduct formation has been explicitly observed and verified to result from the cycloaddition of triplet uracil/thymine with cyclopentene. However, the reaction rate constant can not be determined properly by following either the triplet decay or photoproduct formation due to their relatively poor signals in the transient IR spectra. On the other hand, triplet pyrimidine bases are known to possess strong characteristic absorptions in transient UV–vis spectra.⁴⁰ Thus, we perform transient UV–vis measurements with nanosecond laser flash photolysis to characterize the reaction kinetics of the triplet mediated cycloadditions of these pyrimidine bases.

Transient absorption spectra for uracil and thymine in Ar-saturated acetonitrile are shown in Figures 6 and 7. The strong absorption of the probing light by the ground state pyrimidine bases prevents a study below 300 nm. Transients measured over a broad range of probe wavelengths revealed a band over 300–550 nm immediately after the 266 nm laser excitation. The transient absorption bands show first-order decay kinetics (see Figure 6, inset) independent of the probe wavelength, which means the band is attributed to a single transient. The spectral pattern and peak position matches the reported triplet state spectra of uracil and thymine.⁴⁰ In addition, the transient was efficiently quenched by dissolved oxygen, so the transient is assigned to the lowest excited triplet.

The typical time profiles of the transient absorption at 360 nm for triplet uracil are shown in Figure 6 inset. Due to the photocycloaddition reaction, the decay of the T_1 state transient was significantly accelerated in the presence of cyclopentene. In the transient absorption spectra recorded under these conditions, no new species absorbing in the range 300–550 nm are present. The T_1 state decays were measured for a series of solutions containing uracil or thymine at fixed concentration and the cyclopentene at concentrations ranging from 2 to 14 mM. Pseudo-first-order rate constants (k_{obs}) determined from decay curves are plotted against the concentration of the cyclopentene and shown in the inset of Figure 7. The quenching rate constants of triplet uracil (k_q/Ura) or thymine (k_q/Thy) by cyclopentene can be determined from the slopes of these linear plots, which is $(1.5 \pm 0.06) \times 10^9$ and $(0.6 \pm 0.13) \times 10^9 \text{ M}^{-1} \text{ s}^{-1}$ for uracil and thymine, respectively. These two values are comparable to the known self-quenching rate constant of $2.0 \times 10^9 \text{ M}^{-1} \text{ s}^{-1}$ for triplet uracil and $0.6 \times 10^9 \text{ M}^{-1} \text{ s}^{-1}$ for triplet thymine.⁴⁰

Assuming that the quenching rate constants (k_q/Ura and k_q/Thy) obtained from laser flash photolysis represent the photocycloaddition rate constants, the processes occurring upon UV excitation of pyrimidine bases in the presence of cyclopentene can be described by the following equations, taking uracil as an example.



Under this assumption, the photoproduct quantum yields can be calculated using the equation of $\phi_R = \phi_T k_q/\text{Ura}$

$[\text{R}]/(k_0 + k_{\text{sq}}[\text{Ura}] + k_q/\text{Ura} [\text{R}])$. In the TR-FTIR experiments measuring the photoproduct yields, the concentration of cyclopentene is much larger (100 mM) than that of uracil (0.6 mM), so the calculated photoproduct quantum yield 19.8% is approximately equal to the triplet quantum yields ϕ_T . The photoproduct yield for thymine can be calculated to be 5.9% in the same way. However, compared to those ideal values calculated from rate constants, the reaction quantum yields estimated through the measurement of photoproduct formation in TR-FTIR experiments are much lower, which is 0.91 and 0.41% for the photocycloaddition of uracil or thymine to cyclopentene, respectively. This inefficiency in formation of photoproducts may be the result of competitive physical quenching processes, which do not lead to permanent chemical change. Although the overall quenching rate constants of triplet uracil (or thymine) by cyclopentene is quite large, an efficient energy wasting process may exist on the route leading to stable photoproducts, resulting in very small product yields eventually. Such an energy wasting process is elucidated to be resulted from T_1/S_0 surface crossings in the following theoretical calculations.

3.3. Potential Energy Profiles for [2 + 2] Photocycloaddition Along S_0 , T_1 , and S_1 States. Stationary structures were optimized and potential energy profiles were calculated for the cycloaddition reaction along the S_0 and T_1 states with DFT method at the level of 6-311+G(d,p), which is feasible to explore reactions for larger systems using quantum chemical calculations.³⁰ In parallel, the reaction pathways were also explored on the singlet excited state S_1 on the basis of TD-DFT calculations using the S_0 stationary structures. The calculation results are displayed in Figures 8–10. There are almost identical potential energy profiles for uracil and thymine reacting with cyclopentene, respectively, and only the results for uracil are discussed below as an example. Basically, two stereoisomers of the cyclobutane products, *trans-syn* (P1–S) and *cis-syn* (P2–S) can be yielded from the photocycloaddition with similar reaction routes and our discussion is focused on the formation of the *cis-syn* stereoisomer.

As shown in Figure 9, the [2 + 2] cycloaddition reaction between uracil and cyclopentene on the S_0 surface is a concerted process through one four-membered cyclic transition state. All bond breaking and bond making occurs in a singlet step without any intermediates, yielding the *cis-syn* cyclobutane product (P2–S), which requires surmounting a quite high barrier of 70.3 kcal mol⁻¹. Obviously, the formation of cyclobutane products on ground state is energetically inaccessible at room temperature.

The approximate potential energy profile for the S_1 state obtained by TD-DFT (Figure 9) reveals an energy barrier of 9.3 kcal/mol before the system reaches a potential well. Calculated with a nuclear configuration of the S_0 transition structure (P2-S-TS), this local minimum is 30.4 kcal/mol vertically above P2-S-TS. Such a large energy gap indicates a low possibility for radiationless transition from S_1 to S_0 . Moreover, the subsequent transformation from the potential well to the final product has to overcome a 30.2 kcal/mol barrier (transition state at 130.9 kcal/mol), which is energetically inaccessible for the 266 nm excitation with photon energy of 107 kcal/mol. Therefore, the direct cycloaddition reaction on the S_1 potential surface is infeasible.

Distinctively different from the concerted path on the singlet surface, the reaction follows a stepwise mechanism on the triplet PES as shown in Figure 10. Originated from the $\text{C}=\text{C} \pi \rightarrow \pi^*$ excitation with the $\text{C}\alpha-\text{C}\beta \pi$ -bond (1.357 Å) lengthened to a

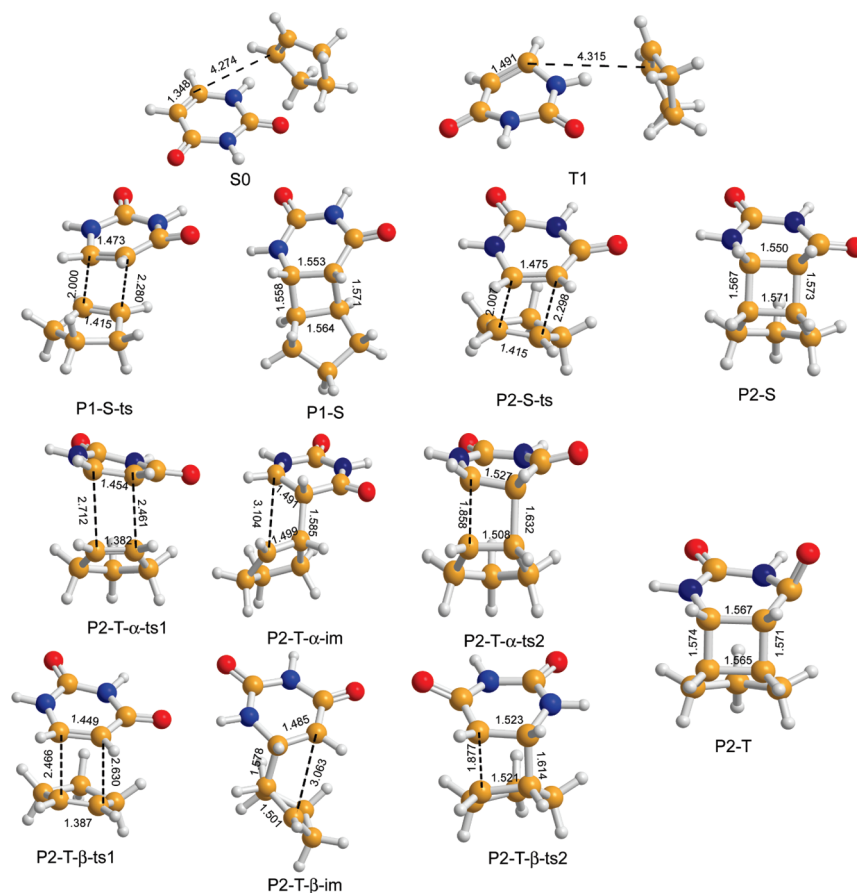


Figure 8. B3LYP/6-311+G(d,p) optimized geometrical parameters of the stationary structures for the uracil–cyclopentene cycloaddition reaction in their singlet ground and triplet states. Bond lengths are in angstrom and bond angles are in degrees. For the reactant complexes, transition structures, and products, all geometries are optimized without any constraints.

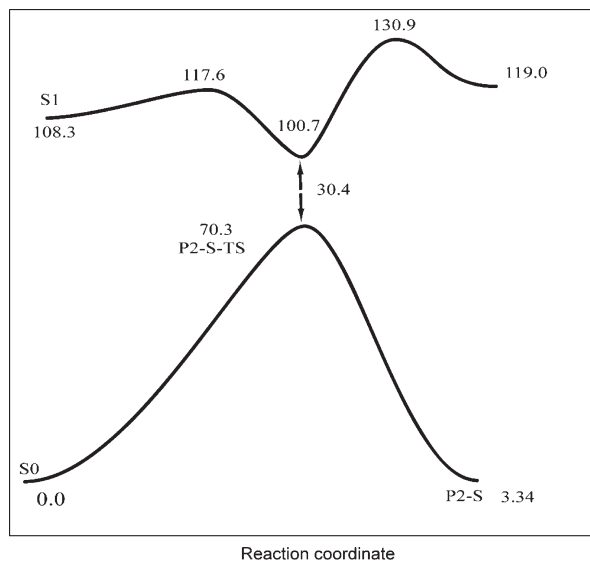


Figure 9. S_0 and S_1 state potential energy profiles along an arbitrary reaction coordinate for the cycloaddition reactions of uracil with cyclopentene. Relative energy values are obtained from the B3LYP/6-311+G(d,p) calculations. The ZPVE corrected total energies are indicated in kcal mol⁻¹.

σ -bond (1.494 Å), the triplet uracil can be envisioned as a biradical with the spin densities localized on the ethylenic $C\alpha$

and $C\beta$ atoms (Note: the $C\alpha$ and $C\beta$ atoms are labeled in Scheme 1, adopting the notation for enones). Thus, the two ethylenic $C\alpha$ and $C\beta$ atoms of triplet uracil become reactive and bond with cyclopentene stepwisely by two pathways which can be described as α -attack pathway and β -attack pathway as follows.

The α -attack pathway (see Figure 10a) proceeds through initial attack of $C\alpha$ on $C\alpha'$, followed by $C\beta$ – $C\beta'$ cross-link formation (route P2-T- α -ts1 \rightarrow P2-T- α -im \rightarrow P2-T- α -ts2 \rightarrow P2-T). Here, $C\alpha$ and $C\beta$ denotes the two ethylenic carbon atoms of triplet uracil, while $C\alpha'$ and $C\beta'$ are the ethylenic carbon atoms of cyclopentene, as indicated in Scheme 1. The initial attack by $C\alpha$ on $C\alpha'$ faces only a barrier of 1.9 kcal/mol, leading to biradical intermediate P2-T- α -im lying 15.3 kcal/mol below the T_1 complex. The first step is quite facile. However, the second step for the $C\beta$ – $C\beta'$ cross-link requires surmounting a high barrier of 51.9 kcal/mol, forming the triplet cyclobutane adduct P2-T, which has a relative energy of 92.9 kcal/mol with respect to the S_0 zero level. Similarly, the other pathway to the formation of cyclobutane adduct P2-T on the triplet PES, that is, the β -attack pathway (see Figure 10b), proceeds through initial attack by $C\beta$ on $C\beta'$ with a barrier of 2.1 kcal/mol, followed by $C\alpha$ – $C\alpha'$ cross-link formation with a barrier of 50.8 kcal/mol (route P2-T- β -ts1 \rightarrow P2-T- β -im \rightarrow P2-T- β -ts2 \rightarrow P2-T).

Considering such high barriers for the biradical intermediates (either P2-T- α -im or P2-T- β -im) to finish the cross-link forming

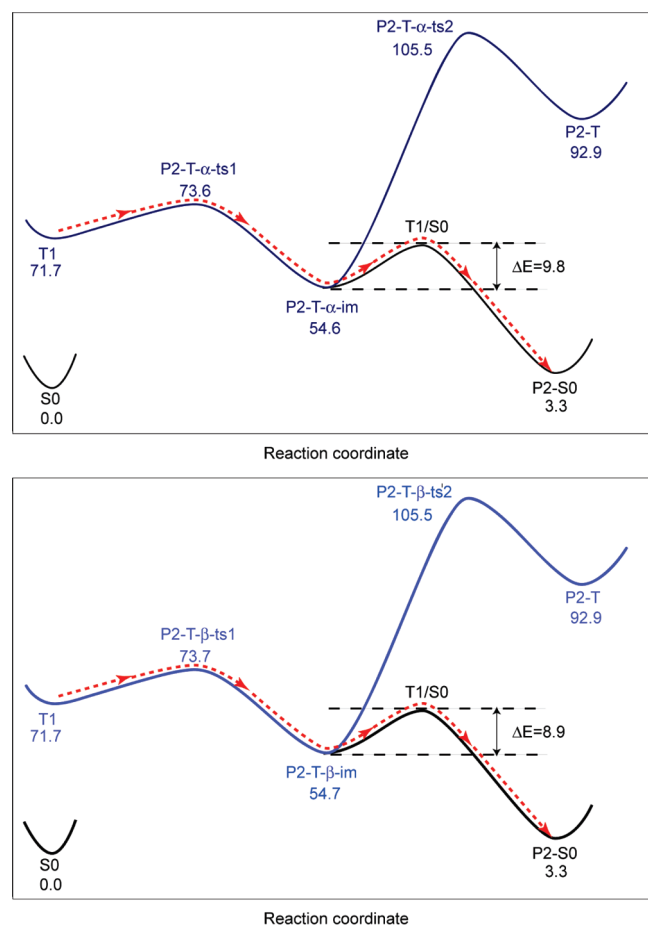


Figure 10. T_1 state potential energy profiles along an arbitrary reaction coordinate for the cycloaddition reactions of uracil with cyclopentene: (a) α -attack pathway; (b) β -attack pathway. Relative energy values are obtained from the B3LYP/6-311+G(d,p) calculations. The ZPVE corrected total energies are indicated in kcal mol⁻¹. The T_1/S_0 surface intersections are located by scanning the relaxed potential energy curves for the two states as shown in Figure 11. The red dotted lines highlight the lowest energy reaction pathways.

final products, there is little possibility that the cycloaddition occurs on the triplet PES only. Possibly, T_1/S_0 surface intersections may exist which lead to intersystem crossing from T_1 to S_0 along the reaction path of ring-closure. To obtain a reliable singlet–triplet interaction profile, the PES for the α -attack pathway was scanned from P2-T- α -im to P2-T- α -ts2 by varying the $C\beta$ – $C\beta'$ distances with a step length of 0.1 Å, constraining the $C\alpha$ – $C\alpha'$ at 1.585 Å and optimizing the remaining coordinates. The same procedure was used to determine the PES for the β -attack pathway from P2-T- β -im to P2-T- β -ts2, fixing $C\beta$ – $C\beta'$ at 1.578 Å and scanning the $C\alpha$ – $C\alpha'$ distance.

The scanned energy profiles are displayed in Figure 11a,b. Clearly, T_1/S_0 surface intersections can be located along the reaction path. For the intermediate P2-T- α -im, with $C\alpha$ – $C\alpha'$ already formed, there is a T_1/S_0 crossing point in the $C\beta$ – $C\beta'$ distance of 2.488 Å with an energy of ca. –610.232668 hartree. The estimated energy gap from P2-T- α -im to the crossing point is approximately 9.8 kcal/mol. Likewise, the T_1/S_0 crossing point along the P2-T- β -im to P2-T- β -ts2 path is found at the $C\alpha$ – $C\alpha'$ distance of 2.487 Å with an energy of approximately 8.9 kcal/mol above P2-T- β -im. For both pathways (α -attack and β -attack),

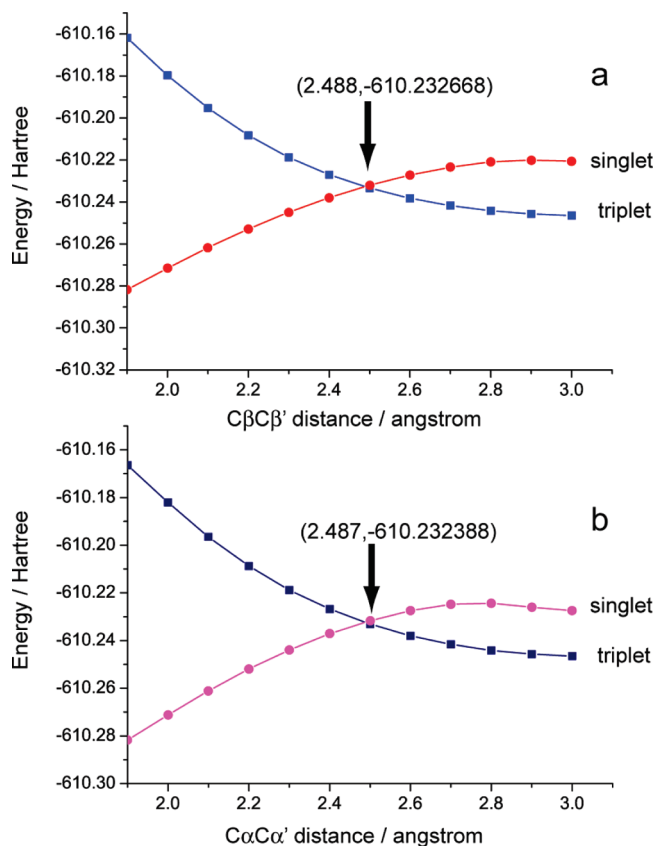


Figure 11. Relaxed potential energy curves for singlet and triplet states along the path from biradical intermediates to full cross-linked photo-products, obtained at the B3LYP/6-311+G(d,p) level: (a) α -attack pathway; (b) β -attack pathway.

the energy barriers from the biradical intermediates to the T_1/S_0 crossing points are dramatically lower than the barriers of 51.9 or 50.8 kcal/mol required to form the triplet cyclobutane adduct P2-T. As a result, once the single cross-linked biradical intermediates (P2-T- α -im and P2-T- β -im) are formed on the triplet PES, the system tends to cross over to the S_0 surface via the T_1/S_0 crossing points and finish the ring-closure process thereafter, leading eventually to the ground state cyclobutane adduct P2-S. Overall, the photocycloaddition reaction should follow such nonadiabatic pathways involving both T_1 and S_0 states, as highlighted with red dotted lines in Figure 10a,b. The nonadiabatic pathways are only rate-limited by the barrier of 9.8 or 8.9 kcal/mol for the triplet biradical intermediates to reach the T_1/S_0 crossing points and thus correspond to the lowest energy path, when compared to all the other adiabatic reaction pathways proceeding through S_1 , T_1 , or S_0 states alone.

In parallel to the photoproduct formation, from the T_1/S_0 crossing points, which is close to the biradical intermediates, the system may also cross over to the ground state reactants, resulting in the S_0 state recovery and a net result of physical quenching instead of chemical transformation. This can explain why the T_1 quenching, though efficient, gives only a very low yield of the cyclobutane photoproduct, as shown in our TR-FTIR and laser flash photolysis experiments. Combined with the experimental observation, it shows here that although the triplet state of pyrimidine bases are highly susceptible to cycloaddition reactions leading to photodamage, the existence of T_1/S_0 crossing points along the T_1 reaction pathway may play important

photoprotective roles by reverting most of the biradical intermediates into two ground state molecules, while transforming only a small fraction into photoproduct.

4. CONCLUSION

Taking the 266 nm excited pyrimidine (uracil or thymine) with cyclopentene as model reaction systems, we have examined the photoproduct formation dynamics from the [2 + 2] photocycloaddition reactions of triplet pyrimidines in solution and provided mechanistic insights into this important DNA photo-damage reaction. Experimentally, nanosecond time-resolved FTIR and UV-vis laser flash-photolysis spectroscopy are combined together to measure the photoproduct formation dynamics as well as the triplet quenching kinetics. Characteristic IR absorption bands due to the cyclobutane photoproduct formation have been observed and product quantum yields are determined to be ~0.91% for uracil and ~0.41% for thymine. Compared to the measured large quenching rate constants of triplet uracil ($1.5 \times 10^9 \text{ M}^{-1} \text{ s}^{-1}$) or thymine ($0.6 \times 10^9 \text{ M}^{-1} \text{ s}^{-1}$) by cyclopentene, the inefficiency in formation of photoproducts indicates competitive physical quenching processes may exist on the route leading to photoproducts, resulting in very small product yields eventually.

Theoretically, potential energy profiles for the cycloaddition reaction along the S_0 , T_1 , and S_1 states are explored with DFT and TD-DFT methods at the level of 6-311+G(d,p) and the T_1/S_0 energy crossing points are located. All the adiabatic reaction pathways proceeding through S_1 , T_1 , or S_0 states alone are shown to be energetically infeasible, while the nonadiabatic pathways involving both T_1 and S_0 states correspond to the lowest energy path and are the most favorable in energy. Combined with the experimental observation, the reaction is elucidated to follow a stepwise triplet mechanism involving the initial formation of a single cross-linked biradical in the T_1 state followed by a cross over to the S_0 surface via the T_1/S_0 crossing points and finish the ring-closure process thereafter. The T_1/S_0 surface intersections lying only 9.8 or 8.9 kcal/mol above the triplet biradical intermediates play significant roles by lowering the energy barriers and facilitating the photoproduct formation via triplet mechanism. On the other hand, the existence of T_1/S_0 crossing points may also play photoprotective roles by reverting most of the biradical intermediates into two ground state reactants, while transforming only a small fraction into photoproducts. This agrees well with our experimental observation that the T_1 quenching, though efficient, gives only a very low quantum yield of the cyclobutane photoproduct.

AUTHOR INFORMATION

Corresponding Author

*E-mail: hongmei@iccas.ac.cn.

ACKNOWLEDGMENT

This work is financially supported by the National Natural Science Foundation of China (Grant Nos. 20733005, 20973179, and 21073201), the National Basic Research Program of China (2007CB815200, 2007AA02Z116), and the Chinese Academy of Sciences.

REFERENCES

- (1) Matsika, S. *J. Phys. Chem. A* **2004**, *108*, 7584.
- (2) Perun, S.; Sobolewski, A. L.; Domcke, W. *J. Phys. Chem. A* **2006**, *110*, 13238.
- (3) Crespo-Hernandez, C. E.; Cohen, B.; Hare, P. M.; Kohler, B. *Chem. Rev.* **2004**, *104*, 1977.
- (4) Merchan, M.; Gonzalez-Luque, R.; Climent, T.; Serrano-Andres, L.; Rodriguez, E.; Reguero, M.; Pelaez, D. *J. Phys. Chem. B* **2006**, *110*, 26471.
- (5) Pecourt, J. M. L.; Peon, J.; Kohler, B. *J. Am. Chem. Soc.* **2000**, *122*, 9348.
- (6) Malone, R. J.; Miller, A. M.; Kohler, B. *Photochem. Photobiol.* **2003**, *77*, 158.
- (7) Pecourt, J. M. L.; Peon, J.; Kohler, B. *J. Am. Chem. Soc.* **2001**, *123*, 10370.
- (8) Peon, J.; Zewail, A. H. *Chem. Phys. Lett.* **2001**, *348*, 255.
- (9) Pancur, T.; Schwalb, N. K.; Renth, F.; Temps, F. *Chem. Phys.* **2005**, *313*, 199.
- (10) Gustavsson, T.; Sarkar, N.; Lazzarotto, E.; Markovitsi, D.; Improta, R. *Chem. Phys. Lett.* **2006**, *429*, 551.
- (11) Rycyna, R. E.; Alderfer, J. L. *Biochemistry* **1988**, *27*, 3142.
- (12) Morrison, H. *Bioorganic Photochemistry: v.1. Photochemistry and the Nucleic Acids*; Wiley: New York, 1990.
- (13) Beukers, R.; Eker, A. P. M.; Lohman, P. H. M. *DNA Repair* **2008**, *7*, 530.
- (14) Sinha, R. P.; Hader, D. P. *Photochem. Photobiol. Sci.* **2002**, *1*, 225.
- (15) Yoon, J. H.; Lee, C. S.; O'Connor, T. R.; Yasui, A.; Pfeifer, G. P. *J. Mol. Biol.* **2000**, *299*, 681.
- (16) Clingen, P. H.; Arlett, C. F.; Roza, L.; Mori, T.; Nikaido, O.; Green, M. H. L. *Cancer Res.* **1995**, *55*, 2245.
- (17) Mouret, S.; Baudouin, C.; Charveron, M.; Favier, A.; Cadet, J.; Douki, T. *Proc. Natl. Acad. Sci. U.S.A.* **2006**, *103*, 13765.
- (18) Turro, N. J. *Modern Molecular Photochemistry*; University Science Books: Herndon, VA, 1978.
- (19) Johns, H. E.; Delbruck, M.; Rapaport, S. A. *J. Mol. Biol.* **1962**, *4*, 104.
- (20) Whillans, D. W.; Johns, H. E. *J. Am. Chem. Soc.* **1971**, *93*, 1358.
- (21) Gustavsson, T.; Banyasz, A.; Lazzarotto, E.; Markovitsi, D.; Scalmani, G.; Frisch, M. J.; Barone, V.; Improta, R. *J. Am. Chem. Soc.* **2006**, *128*, 607.
- (22) Schreier, W. J.; Schrader, T. E.; Koller, F. O.; Gilch, P.; Crespo-Hernandez, C. E.; Swaminathan, V. N.; Carell, T.; Zinth, W.; Kohler, B. *Science* **2007**, *315*, 625.
- (23) Martinez, J. M.; Elmroth, S. K. C.; Kloo, L. *J. Am. Chem. Soc.* **2001**, *123*, 12279.
- (24) Schreier, W. J.; Kubon, J.; Regner, N.; Haiser, K.; Schrader, T. E.; Zinth, W.; Clivio, P.; Gilch, P. *J. Am. Chem. Soc.* **2009**, *131*, 5038.
- (25) Boggio-Pasqua, M.; Groenhof, G.; Schafer, L. V.; Grubmuller, H.; Robb, M. A. *J. Am. Chem. Soc.* **2007**, *129*, 10996.
- (26) Hare, P. M.; Crespo-Hernandez, C. E.; Kohler, B. *Proc. Natl. Acad. Sci. U.S.A.* **2007**, *104*, 435.
- (27) Hare, P. M.; Crespo-Hernandez, C. E.; Kohler, B. *J. Phys. Chem. B* **2006**, *110*, 18641.
- (28) Mills, J. B.; Vacano, E.; Hagerman, P. J. *J. Mol. Biol.* **1999**, *285*, 245.
- (29) Kwok, W. M.; Ma, C.; Phillips, D. L. *J. Am. Chem. Soc.* **2008**, *130*, 5131.
- (30) Zhang, R. B.; Eriksson, L. A. *J. Phys. Chem. B* **2006**, *110*, 7556.
- (31) Hare, P. M.; Middleton, C. T.; Mertel, K. I.; Herbert, J. M.; Kohler, B. *Chem. Phys.* **2008**, *347*, 383.
- (32) Uhmman, W.; Becker, A.; Taran, C.; Siebert, F. *Appl. Spectrosc.* **1991**, *45*, 390.
- (33) Drapcho, D. L.; Curbelo, P. E.; Jiang, Y.; Crocombe, R. A.; McCarthy, W. J. *Appl. Spectrosc.* **1997**, *54*, 453.
- (34) Frisch, M. J. T., G., W.; Schlegel, H. B.; Scuseria, G. E.; Robb, M. A.; Cheeseman, J. R.; Montgomery, J. A., Jr.; Vreven, T.; Kudin, K. N.; Burant, J. C.; Millam, J. M.; Iyengar, S. S.; Tomasi, J.; Barone, V.; Mennucci, B.; Cossi, M.; Scalmani, G.; Rega, N.; Petersson, G. A.; Nakatsuji, H.; Hada, M.; Ehara, M.; Toyota, K.; Fukuda, R.; Hasegawa,

J.; Ishida, M.; Nakajima, T.; Honda, Y.; Kitao, O.; Nakai, H.; Klene, M.; Li, X.; Knox, J. E.; Hratchian, H. P.; Cross, J. B.; Bakken, V.; Adamo, C.; Jaramillo, J.; Gomperts, R.; Stratmann, R. E.; Yazyev, O.; Austin, A. J.; Cammi, R.; Pomelli, C.; Ochterski, J. W.; Ayala, P. Y.; Morokuma, K.; Voth, G. A.; Salvador, P.; Dannenberg, J. J.; Zakrzewski, V. G.; Dapprich, S.; Daniels, A. D.; Strain, M. C.; Farkas, O.; Malick, D. K.; Rabuck, A. D.; Raghavachari, K.; Foresman, J. B.; Ortiz, J. V.; Cui, Q.; Baboul, A. G.; Clifford, S.; Cioslowski, J.; Stefanov, B. B.; Liu, G.; Liashenko, A.; Piskorz, P.; Komaromi, I.; Martin, R. L.; Fox, D. J.; Keith, T.; Al-Laham, M. A.; Peng, C. Y.; Nanayakkara, A.; Challacombe, M.; Gill, P. M. W.; Johnson, B.; Chen, W.; Wong, M. W.; Gonzalez, C.; Pople, J. A. *Gaussian 03*, Revision B.03; Gaussian, Inc.: Wallingford, CT, 2004.

(35) Becke, A. D. *J. Chem. Phys.* **1993**, *98*, 5648.

(36) Lee, C.; Yang, W.; Parr, R. G. *Phys. Rev. B: Condens. Matter* **1988**, *37*, 785.

(37) Gonzalez, C.; Schlegel, H. B. *J. Phys. Chem.* **1990**, *94*, 5523.

(38) Stratmann, R. E.; Scuseria, G. E.; Frisch, M. J. *J. Chem. Phys.* **1998**, *109*, 8218.

(39) Vanderlu, Wt; Oosterho., Lj *J. Am. Chem. Soc.* **1969**, *91*, 6042.

(40) Salet, C.; Bensasson, R. *Photochem. Photobiol.* **1975**, *22*, 231.

(41) Lamola, A. A.; Mittal, J. P. *Science* **1966**, *154*, 1560.

(42) Varghese, A. J. *Biochemistry* **1971**, *10*, 4283.

(43) Jennings, B. H.; Pastra-Landis, S.; Lerman, J. W. *Photochem. Photobiol.* **1972**, *15*, 479.

(44) <http://webbook.nist.gov/>.

(45) Watson, F. H.; McGlynn, S. P. *Theor. Chim. Acta* **1971**, *21*, 309.

(46) Wagner, P. J.; Bucheck, D. J. *J. Am. Chem. Soc.* **1970**, *92*, 181.